EPJ Web of Conferences **364**, 15012 (2026) https://doi.org/10.1051/epjconf/202636415012
Quark Matter 2025

A non-fluctuational signature of the QCD critical point

Maneesha Sushama Pradeep[1,*], *Noriyuki* Sogabe[2,3,4,**], *Mikhail* Stephanov[3,4,***], and *Ho-Ung* Yee[3,4,****]

[1]Department of Physics, University of Maryland, College Park, Maryland 20742, USA
[2]Department of Physics, University of Osaka, Toyonaka, Osaka 560-0043, Japan
[3]Department of Physics, University of Illinois, Chicago, Illinois 60607, USA
[4]Laboratory for Quantum Theory at the Extremes, University of Illinois, Chicago, Illinois 60607, USA

Abstract. We propose a novel, non-fluctuational signature of the QCD critical point, originating from hydrodynamic trajectories that bend toward the maximum of the specific entropy per baryon along the chiral phase transition boundary. Specifically, if the critical point lies sufficiently close to the freeze-out points, the freeze-out chemical potential may exhibit a discontinuous jump as a function of the collision energy.

1 Introduction

Understanding the phase structure of Quantum Chromodynamics (QCD) at finite temperature T and baryon chemical potential μ is a central aim of the Relativistic Heavy Ion Collider (RHIC). A key target is the QCD critical point, where the smooth crossover turns into the first-order chiral phase boundary between hadron resonance gas (HRG) and the quark-gluon plasma (QGP). The STAR Collaboration's recent measurements of baryon-number fluctuations in the Beam Energy Scan II (BES-II) program [1] qualitatively agree with expectations for a critical point at $\mu \gtrsim 420\,\mathrm{MeV}$ (see Ref. [2] for a review). To make a quantitative comparison between theory and experiment, one must understand how these fluctuations evolve and freeze out during the hydrodynamic expansion of the fireball. The theoretical framework for describing the time-evolution of (non-Gaussian) fluctuations has been developed using a stochastic diffusion approach [3] together with a non-equilibrium effective field theory on the Schwinger-Keldysh contour [4].

Ideal hydrodynamics provides the leading-order description of the fireball's evolution. In this approximation, the specific entropy per bayon number, $\hat{s} \equiv s/n$ is conserved, so the system evolves along isentropic curves on the (μ, T) plane defined by $\hat{s}(\mu, T) = \hat{s}_0$ with $\hat{s}_0$ determined by the initial state. Since the equation of state (EOS) near the QCD critical point can be mapped onto that of the 3D Ising model, the shape of these isentropic trajectories may encode universal features from the critical EOS, which we shall discuss below, along with their consequences for the freeze-out points.

*e-mail: mpradeep@umd.edu
**e-mail: nori.sogabe@gmail.com
***e-mail: misha@uic.edu
****e-mail: hyee@uic.edu

2 Non-monotonic specific entropy and its geometric consequences

2.1 Non-monotonic specific entropy

In our previous work [5], we found a universal non-monotonic behavior of the specific entropy along the first-order phase boundary as shown in Fig. 1(a). The maximum $\hat{s} = \hat{s}_{\max}$ (green point) emerges from the interplay between criticality and the third law of thermodynamics (see Ref. [5] for details). It must occur on either the HRG or QGP side (as denoted by phase 1), depending on the sign of the isochoric temperature derivative of the pressure at the critical point, i.e., HRG phase if $(\partial P/\partial T)_{n,\mathrm{c}} > 0$; QGP phase if $(\partial P/\partial T)_{n,\mathrm{c}} < 0$.

2.2 Geometric consequences

This non-monotonic behavior leads to a new geometrical feature of isentropes in the vicinity of the QCD critical point. Figure 1(b) shows representative crossover-type isentropes (pink curves), labeled by different initial values of the specific entropy, $\hat{s}_1 > \cdots > \hat{s}_5 > \hat{s}_{\max}$. As $\hat{s}$ decreases, each trajectory bends toward the maximum point (green marker), following the characteristic magenta "ridge" curve.

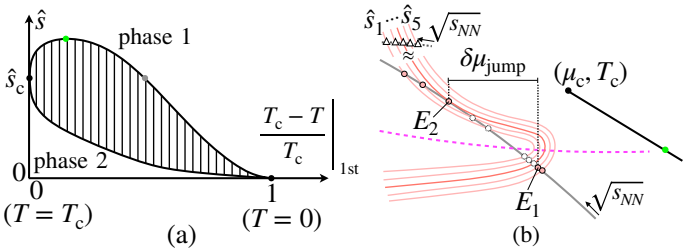

Figure 1. A schematic illustration of (a) the specific entropy (per baryon number) on the coexistence line (first-order phase transition) and (b) the isentropes near the QCD critical point at (μ_c, T_c). Two branches—phases 1 and 2—correspond to the HRG and QGP phases, or vice versa. Panel (b) depicts the case in which phase 1 is the HRG phase, i.e., $(\partial P/\partial T)_{n,\mathrm{c}} > 0$.

3 Freeze-out chemical potential jump

We investigate the impact of these hydrodynamic trajectories on experimental observables. In Fig. 1(b), the gray curve shows the empirical freeze-out curve, obtained by fitting the available freeze-out data. The small circles—filled or open—mark its intersections with different isentropes. If the critical point lies close to this curve, the bending of the isentropes can produce multiple intersections; however, during an adiabatic expansion, the first intersection in time (filled circles) is physically realized. The remaining intersections (open circles) define a region of the freeze-out curve that is inaccessible under isentropic processes. Consequently, as the collision energy $\sqrt{s_{NN}}$ varies, the freeze-out chemical potential exhibits a sudden jump $\delta\mu_{\mathrm{jump}}$, offering a potential *non-fluctuational* signature of the critical point.

For demonstration, we employ $\hat{s}(\mu, T)$ near the critical point [5]; see that reference for its derivation from the 3D Ising EOS. Throughout this work, we chose the mapping parameter between QCD and Ising model as $\alpha_1 = 4.7°$, $\alpha_2 = -3°$, $w = 1.0$, $\rho = 2.0$, $\mu_c = 430\,\mathrm{MeV}$, and $T_c = 140.4\,\mathrm{MeV}$. In addition, we adopt the parametrization of the freeze-out temperature T_f and baryon chemical potential μ_f in Ref. [6]: $T_f(\sqrt{s_{NN}}) = T_{f0}/[1 + \exp(a - b \ln \sqrt{s_{NN}})]$

and $\mu_{\rm f}(\sqrt{s_{NN}}) = \mu_{\rm f0}/(1 + c\sqrt{s_{NN}})$, with $T_{\rm f0} = 158.4\,{\rm MeV}$, $\mu_{\rm f0} = 1307.5\,{\rm MeV}$, $a = 2.60$, $b = 2.22$, and $c = 0.288$. Eliminating $\sqrt{s_{NN}}$ from these equations yields the freeze-out curve, $T_{\rm f}(\mu_{\rm f}) = T_{\rm f0}/\{1 + \exp[a - b\ln(\frac{\mu_{\rm f0}-\mu_{\rm f}}{c\mu_{\rm f}})]\}$.

We denote the n th intersections between a given isentrope $\hat{s}(\mu, T) = \hat{s}_0$ and the freeze-out curve $T = T_{\rm f}(\mu)$ by $X^{(n)}_{\hat{s}_0} \equiv (\mu^{(n)}_{\hat{s}_0}, T^{(n)}_{\hat{s}_0})$, where $n = 1, 2, ...$ is time-ordered so that the entropy density decreases along the trajectory: $s(X^{(1)}_{\hat{s}_0}) > s(X^{(2)}_{\hat{s}_0}) > \cdots$. By scanning $\hat{s}_0$ over the range $\hat{s}_{0,\rm min} \le \hat{s}_0 \le \hat{s}_{0,\rm max}$, we obtain $\hat{s}_0$ dependence of the first intersection, $X^{(1)}(\hat{s}_0)$, which may exibit a sudden jump at some value $\hat{s}_0 = \hat{s}_{0,\rm jump}$ (corresponding to the dark isentrope in Fig. 1(b)). Focusing on the chemical potential, Fig. 2(a) shows $\mu = \mu^{(1)}(\hat{s}_0)$. Pink, purple, and light-blue points classify trajectories that undergo (I) crossover, (II) HRG–HRG, and (III) QGP–HRG transitions, respectively (using the same color notation as Fig. 8 of Ref. [5]).

To reparametrize Fig. 2(a) in terms of experimentally relevant $\sqrt{s_{NN}}$, one might naively employ the mapping determined by the first intersection points,

$$\mu_{\rm f}(\sqrt{s_{NN}}) = \mu^{(1)}(\hat{s}_0) \quad \Rightarrow \quad \hat{s}_0 = \hat{s}_{\rm f}(\sqrt{s_{NN}})\,, \tag{1}$$

where its inverse map is shown by colored points in Fig. 2(b). However, this mapping leaves the interval $E_1 < \sqrt{s_{NN}} < E_2$ (red points) uncovered; since no valid initial states exist there, this map is therefore inadequate for our purposes.

Instead, we introduce a mapping $\hat{s}_0 = \hat{s}_{\rm i}(\sqrt{s_{NN}})$ that spans the full collision-energy range while reproducing the experimental data. We assume that the initial states (triangles in Fig. 1(b)) lie on a smooth curve parametrized by $\sqrt{s_{NN}}$, $T_{\rm i} = T_{\rm i}(\sqrt{s_{NN}})$ and $\mu_{\rm i} = \mu_{\rm i}(\sqrt{s_{NN}})$, as indicated by the gray dotted curve in Fig. 1(b). The function $\hat{s} = \hat{s}_{\rm i}(\sqrt{s_{NN}})$ may be interpreted as the specific entropy along this curve of initial states. Its inverse $(\sqrt{s_{\rm NN}})_{\rm i}(\hat{s}_0)$ is shown as the black curve in Fig. 2(b) and is defined by

$$(\sqrt{s_{\rm NN}})_{\rm i}(\hat{s}_0) = [1 - f(\hat{s}_0)](\sqrt{s_{\rm NN}})^{<}_{\rm f}(\hat{s}_0) + f(\hat{s}_0)(\sqrt{s_{\rm NN}})^{>}_{\rm f}(\hat{s}_0)\,, \tag{2}$$

where $f(\hat{s}_0) = (1 + \tanh[(\hat{s}_0 - \hat{s}_{0,\rm jump} - \Delta\hat{s}_{01})/\Delta\hat{s}_{02}])/2$ is a swtiching function, and the inverse maps $(\sqrt{s_{\rm NN}})^{<}_{\rm f}(\hat{s}_0)$ and $(\sqrt{s_{\rm NN}})^{>}_{\rm f}(\hat{s}_0)$ are defined on $\sqrt{s_{\rm NN}} \le E_1$ and $\sqrt{s_{\rm NN}} \ge E_2$, respectively.

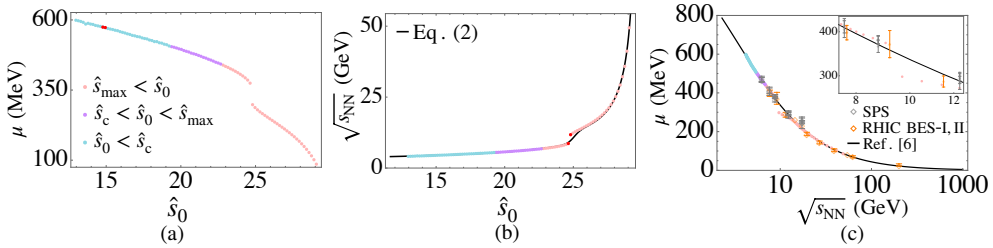

Figure 2. (a) Chemical potential $\mu = \mu^{(1)}(\hat{s}_0)$ and (b) the corresponding collision energy $(\sqrt{s_{NN}})^{<}_{\rm f}(\hat{s}_0)$ for $\hat{s}_0 < \hat{s}_{0,\rm jump}$ and $(\sqrt{s_{NN}})^{>}_{\rm f}(\hat{s}_0)$ for $\hat{s}_0 > \hat{s}_{0,\rm jump}$, evaluated at the intersection points between isentropes of fixed specific entropy $\hat{s} = \hat{s}_0$ and the freeze-out curve. The red points indicate the jump at $\hat{s}_0 \simeq \hat{s}_{0,\rm jump} \approx 24.7$, where in panel (a) μ changes from 375 MeV to 298 MeV, and in pannel (b), $\sqrt{s_{NN}}$ jumps from $E_1 \approx 8.6$ GeV to $E_2 \approx 11.8$ GeV. While the collision energy determined by the intersection points are missing between the red points, we introduce a smooth function (black curve) given by (2) with $\Delta\hat{s}_{01} = 0.4$ and $\Delta\hat{s}_{02} = 0.5$ that spans the entire collision-energy range. This function is used to translate $\hat{s}_0$ variable in panel (a) to $\sqrt{s_{NN}}$. (c) Collision energy dependence of freeze-out chemical potential with our theoretical calculation using the 3D Ising EOS mapped onto QCD (see a parameter choice in text).

Finally, by varying $\hat{s}_0$, we compute the pairs $(\mu, \sqrt{s_{NN}}) = (\mu^{(1)}(\hat{s}_0), \sqrt{s_{NN\rm i}}(\hat{s}_0))$ and obtain the collision energy dependence of the freeze-out chemical potential as shown in Fig. 2(c).

Here, we have overlaid the experimental measurements (orange and gray diamonds with error bars) with the empirical freeze-out fit from Ref. [6]. Plots in the range $E_1 < \sqrt{s_{NN}} < E_2$ is produced by filling the gap between the red points in Fig. 2(b) in use of (2), thus model dependent. Nevertheless, the presence and magnitude of the discontinuity (vertical jump) originally shown in Fig. 2(a), remain topologically robust and model-independent.

The largest experimental gap in μ occurs between 355 MeV at $\sqrt{s_{NN}} = 9.2$ GeV and 287 MeV at $\sqrt{s_{NN}} = 11.5$ GeV, implying $\delta\mu_{\rm jump} \lesssim 70$ MeV, which limits the ranges of the mapping parameters between QCD and 3D Ising model. We have chosen our mapping parameters to produce a jump within this bound. The corresponding temperature jump $\delta T_{\rm jump} \approx 7.5$ MeV is comparable to current experimental error bars and therefore difficult to distinguish. For this reason, we do not present any examples of the freeze-out temperature. If any data at intermediate energies ($9.2\,\text{GeV} < \sqrt{s_{NN}} < 11.5\,\text{GeV}$) confirm such a vertical jump in μ, it would serve as a non-fluctuational signature of the QCD critical point.

4 Conclusion and Outlook

The QCD critical point significantly reshapes the hydrodynamic trajectories of the expanding fireball in heavy-ion collisions, causing them to bend toward the point on the first-order phase boundary where the specific entropy (per baryon) is maximized. We have shown that this geometric feature becomes manifest in the freeze-out points: if the critical point lies close to the freeze-out curve—as is often assumed—adiabatic expansion makes part of that curve inaccessible. Consequently, the collision-energy parametrization of the freeze-out temperature and chemical potential acquires a physical discontinuity. This jump provides a novel, non-fluctuational signature of the critical point, requiring fewer events than conventional fluctuation observables such as cumulants. We have demonstrated the chemical potential jump using a simplified ideal-hydrodynamic model with a QCD equation of state mapped onto the 3D Ising model. While our analysis here focuses on crossover-type isentropes, trajectories that cross the first-order phase boundary are currently under investigation.

This work is supported by the U.S.Department of Energy, Office of Science, Office of Nuclear Physics Award No. DE-FG0201ER41195. M.P. is supported by the U.S. Department of Energy, Office of Nuclear Physics under Award No. DE-FG02-93ER40762.

References

[1] A. Pandav (STAR Collaboration), plenary talk at Critical Point and Onset of Deconfinement (CPOD) 2024

[2] M. Stephanov, QCD critical point: Recent developments, EPJ Web Conf. **314**, 00042 (2024), 2410.02861. 10.1051/epjconf/202431400042

[3] X. An, G. Başar, M. Stephanov, H.U. Yee, Evolution of Non-Gaussian Hydrodynamic Fluctuations, Phys. Rev. Lett. **127**, 072301 (2021), 2009.10742. 10.1103/PhysRevLett.127.072301

[4] N. Sogabe, Y. Yin, Off-equilibrium non-gaussian fluctuations near the qcd critical point: an effective field theory perspective, Journal of High Energy Physics **2022**, 124 (2022). 10.1007/JHEP03(2022)124

[5] M.S. Pradeep, N. Sogabe, M. Stephanov, H.U. Yee, Nonmonotonic specific entropy on the transition line near the QCD critical point, Phys. Rev. C **109**, 064905 (2024), 2402.09519. 10.1103/PhysRevC.109.064905

[6] A. Andronic, P. Braun-Munzinger, K. Redlich, J. Stachel, Decoding the phase structure of QCD via particle production at high energy, Nature **561**, 321 (2018), 1710.09425. 10.1038/s41586-018-0491-6